Spin-Orbit Coupling corrections for the GFN-xTB method

Gautam Jha,[1,2] Thomas Heine[1,2,3,]*

[1]Helmholtz-Zentrum Dresden-Rossendorf, Institut für Ressourcenökologie, Bautzner Landstraße 400, 01328 Dresden

[2]TU Dresden, Fakultät für Chemie und Lebensmittelchemie, Bergstraße 66c, 01062 Dresden, Germany

[3]Department of Chemistry, Yonsei University, Seodaemun-gu, Seoul 120-749, Republic of Korea

*thomas.heine@tu-dresden.de

ABSTRACT

Spin-orbit coupling (SOC) is crucial for correct electronic structure analysis in molecules and materials, for example in large molecular systems as in superatoms, for understanding the role of transition metals in enzymes, and when investigating the energy transfer processes in metal-organic frameworks. We extend the GFN-xTB method, popular to treat extended systems, by including SOC into the hamiltonian operator. We followed the same approach as previously reported for the density-functional tight-binding (DFTB) method and provide and validate the necessary parameters for all elements throughout the periodic table. The parameters have been

obtained consistently from atomic SOC calculations using density-functional theory. We tested them for reference structures where SOC is decisive, as in transition metal containing heme moiety, chromophores in metal-organic frameworks, and in superatoms. Our parametrization paves the path for incorporation of SOC in GFN-xTB based electronic structure calculations of computationally expensive molecular systems.

Introduction

Density-functional Theory (DFT) is a computationally feasible first principles method known for its chemical accuracy and computational scalability [1,2]. However, most of the fascinating chemistry occurring at the biochemical and material level incorporates thousands of atoms. Metallo-proteins, metal-organic frameworks (MOFs), superatoms, and nanoclusters involve thousands of atoms. GFN-xTB [3,4], an advanced semi-empirical quantum mechanical method, has proven its usefulness in describing the chemistry and physics of such large molecular [3,5] and periodic [6] systems. To date, all extensions of GFN-xTB are formulated in a spin-restricted way, and only consider scalar relativistic effects in form of effective core potentials, but do not account for spin-orbit coupling (SOC) [7]. Here, we incorporate SOC into the GFN1-xTB method following the same approach as in density-functional based tight-binding (DFTB) [8]. Our approach for incorporation of SOC to GFN1-xTB is transferrable to other extensions of GFN-xTB, such as GFN2-xTB, and possible future versions. We provide parameters covering the elements throughout the periodic table [9], and validate them with typical molecular benchmark systems.

SOC is a relativistic effect originating from the Dirac equation, a relativistic analogue of the Schrödinger equation (SE). SOC can be added to the hamiltonian operator through approximate decoupling of a fully relativistic Dirac equation in 2-components and then splitting scalar and

SOC parts. This can be performed, for example, by using the exact two component (X2C) method, the zeroth order regular approximation (ZORA) [10,11], or the Douglas-Kroll-Hess (DKH) approximation [12]. Semi-empirical quantum mechanical methods solve the SE, and relativistic corrections can be added to it in two parts. First, the inertial mass of the electrons is corrected via pseudopotentials or by employing ZORA. One important fact to be mentioned here is that the mass-velocity correction for the s electrons gets counteracted by the Darwin term. Second, by coupling of the spin of the electron with the magnetic field in the reference frame of electron, known as SOC [13].

SOC is crucial for electronic structure analysis of many molecular systems. SOC perturbs the electronic structure of molecules and accounts for various interesting properties. One example are MOFs, an emerging materials class with applications, among others, in energy applications including the photochemical conversion of solar energy. Studies concerning the effect of SOC[14] on the absorption spectra of complexes such as in $M(bpy)_3^{2+}$ (M = Fe, Ru, Os ; bpy = 2,2' -Bipyridine) have facilitated the research on understanding of energy transfer processes in MOFs.[15,16] Similarly, Chakraborty et al. emphasized the effect of SOC in dipole-dipole energy transfer in Ru(II), Ir(III), and Os(II) polypyridyl complexes incorporated into the backbone of the MOF UiO-67 [17].

Superatoms are an exciting class of clusters with free-atom-like properties, and thus can serve as building blocks for advanced nanomaterials [18,19]. Assemblies of ligated magnetic superatoms can serve as better molecular electronic devices, as weak fields can control the coupling [20], SOC can affect the electron affinity of superatoms to a great extent, as for example in $[WAu_{12}]$ with an electron affinity difference of ~2 eV [21], which affects the charge transfer process.

Enzymes have manifested themselves as vital elements of the biosphere and have contributed to the advent of life in its current form. Enzymatic processes as in binding of oxygen to

hemoglobin and myoglobin are supposed to be of low yield, as for example the reaction between singlet O_2 and quintet heme moiety is spin-forbidden. Presence of transition metals in the enzymes lifts the spin prohibition [22], as SOC results in mixing of the states. Hence, SOC is crucial for correctly describing the high yield in one of the most important biological process, binding of oxygen to hemoglobin. Similarly, SOC affects the yield of final products in various chemical process, such as spin catalysis.[23–25] SOC also facilitates the singlet to triplet intersystem crossing in systems containing heavy compounds [24]. Thus, a proper account of SOC in chemical reactions is crucial for the correct prediction of the yield of end products.

As SOC is a physical effect impacting various electronic and transport properties of extended molecules and molecular framework materials, it makes a very useful and timely addition to the GFN-xTB approaches. One can extend the GFN-xTB hamiltonian to include a SOC correction based on an atom-dependent parametrization with similar computational cost as of a non-collinear spin-polarized calculation. One limit of such implementations is the availability of accurate SO splitting parameters throughout the periodic table, which was overcome in our previous work [9].

In the present study, we have implemented the SOC extension within the LS coupling model to GFN1-xTB, using exactly the same approach as earlier reported for DFTB [8,9]. We validated approach and parameters on a variety of reference structures, including chromophores in MOFs, superatoms, and transition metal containing heme moieties. We calculated the spin-orbit splitting of valence molecular orbitals and compared with the reference values calculated at DFT level with SOC-ZORA relativistic corrections. We observed excellent agreement between both methods, the error bar of our SOC correction is typically lower than that expected for the molecular orbitals.

Method

In this section, we give the SOC extension to the GFN-xTB method and the calculation of parameters that will be included into the model. While we have implemented it here both for GFN1-xTB and GFN2-xTB, we concentrated us in the tests in the more wide-spread GFN1-xTB variant. Extension and parameterization are identical to our previous work on DFTB [9] and are included here for completeness.

Extended Tight-Binding method. The total energy in GFN1-xTB [4] comprises electronic energy (E_{el}), atom-pairwise repulsion (E_{rep}), dispersion (E_{disp}), and halogen bonding term (E_{XB}) which is represented as:

$$E_{GFN-xTB} = E_{el} + E_{rep} + E_{disp} + E_{XB} \qquad ..Eq(1)$$

The electronic energy is given as:

$$E_{el} = \sum_{i}^{occ.} n_i \langle \psi_i | H_0 | \psi_i \rangle + \frac{1}{2} \sum_{A,B} \sum_{l(A)} \sum_{l'(B)} p_l^A p_{l'}^B \gamma_{AB,ll'} + \frac{1}{3} \sum_{A} \Gamma_A q_A^3 - T_{el} S_{el} \qquad ..Eq(2)$$

where H_0 is the zero-order hamiltonian, ψ_i is the single-electron wave function of a valence molecular orbital (MO), and n_i is the occupation number of MO of index i. Second and third terms comprise the self-consistent charge (SCC) contributions to the electronic energy. q_A is the Mulliken charge of atom A and Γ_A is the charge derivative of the atomic Hubbard parameter. $T_{el}S_{el}$ is the electronic free energy of the system. A and B are two distinct atoms of the system, l and l' are orbital angular momentums of the atomic shells of atoms A and B, respectively. p_l^A is the charge distributed over the atomic shell with orbital angular momentum number l at atom A. The distance dependence of the Coulomb interaction is given as $\gamma_{AB,ll'}$ following the generalized Mataga-Nishimoto-Ohno-Klopman formalism [26–29]. A detailed description of GFN1-xTB formalism is provided in the SI.

SOC incorporation to the GFN1-xTB hamiltonian in LS coupling model [13] is given as:

$$\widehat{H}_{\mu\nu}^{\hat{L}\cdot\hat{S}} = \frac{1}{2} S_{\mu\nu}\left[\epsilon_\mu \begin{pmatrix} \hat{L}_Z & \hat{L}_- \\ \hat{L}_+ & -\hat{L}_Z \end{pmatrix} + \epsilon_\nu \begin{pmatrix} \hat{L}_Z & \hat{L}_- \\ \hat{L}_+ & -\hat{L}_Z \end{pmatrix}\right] \text{with } \mu \in l \in A, \nu \in l' \in B, \quad ..Eq(3)$$

where μ and ν are atomic shell labels for corresponding AOs with angular momentum l at atom A and l' at atom B. Here ϵ is the SOC parameter, $\hat{L}$ is the angular momentum operator, and $\hat{S}$ is the spin operator. $\widehat{H}_{\mu\nu}^{\hat{L}\cdot\hat{S}}$ is the hamiltonian matrix for dual SOC, where dual stands for considering the off-site corrections in addition to on-site corrections[30].

The full GFN1-xTB Hamiltonian matrix with consideration of spin polarization and SOC [8] reads as:

$$\begin{aligned} H_{\mu\nu} = {} & K_{AB}\frac{1}{2}(k_l + k_{l'})\frac{1}{2}\left(h_A^l + h_B^{l'}\right)S_{\mu\nu}(1 + k_{EN}\Delta EN_{AB}^2)\Pi\left(R_{AB,ll'}\right)\begin{pmatrix} 1 & 0 \\ 0 & 1 \end{pmatrix} \\ & + \frac{1}{2}S_{\mu\nu}\sum_C\sum_{l''}\left(\gamma_{AC,ll''} + \gamma_{BC,l'l''}\right)p_{l''}^C\begin{pmatrix} 1 & 0 \\ 0 & 1 \end{pmatrix} + \frac{1}{2}S_{\mu\nu}(q_A^2\Gamma_A + q_B^2\Gamma_B)\begin{pmatrix} 1 & 0 \\ 0 & 1 \end{pmatrix} \\ & \pm \frac{S_{\mu\nu}}{2}\left(\sum_{l''\in A} W_{All''}\begin{pmatrix} p_{Al''}^z & p_{Al''}^y - p_{Al''}^x \\ p_{Al''}^y + p_{Al''}^x & -p_{Al''}^z \end{pmatrix}\right. \\ & \left. + \sum_{l''\in B} W_{Bll''}\begin{pmatrix} p_{Bl''}^z & p_{Bl''}^y - p_{Bl''}^x \\ p_{Bl''}^y + p_{Bl''}^x & -p_{Bl''}^z \end{pmatrix}\right) \\ & + \frac{S_{\mu\nu}}{2}\left[\epsilon_\mu \begin{pmatrix} \hat{L}_Z & \hat{L}_- \\ \hat{L}_+ & -\hat{L}_Z \end{pmatrix} + \epsilon_\nu \begin{pmatrix} \hat{L}_Z & \hat{L}_- \\ \hat{L}_+ & -\hat{L}_Z \end{pmatrix}\right] \mu \in l \in A, \nu \in l' \\ & \in B \qquad ..Eq(4) \end{aligned}$$

Here, k_l and $k_{l'}$ are the Hückel parameters for angular momentum l for atom A and l' for atom B, and K_{AB} is a scaling constant. Energy levels for atom A and atom B are represented as h_A^l and $h_B^{l'}$ with l and l' angular momentum respectively. $S_{\mu\nu}$ is the overlap matrix and ΔEN_{AB} is electronegativity difference of two atoms with k_{EN} as a proportionality coefficient. $\Pi\left(R_{AB,ll'}\right)$ is a distance and l-dependent function.

Calculation of SOC Parameters. We have calculated the SOC parameters for free atoms throughout the periodic table employing AMS-BAND [31] software with two-component relativistic corrections at SOC-ZORA level and TZ2P basis set with all electron approach and then renormalized, as reported earlier [9]. We will, for completeness, briefly outline the approach below. All elements are in their ground state atomic configuration.

Spin-orbit potential, ΔH in terms of ΔH_T (Thomas precession energy) and ΔH_L (Larmor interaction energy) can be given as:

$$\Delta H = \Delta H_T + \Delta H_L = \left(2 - \frac{2\gamma^3}{\gamma + 1}\right) \frac{\mu_B}{\hbar m_e e c^2} \frac{1}{r} \frac{\partial U(r)}{\partial r} L \cdot S \quad ..Eq(5)$$

Where $\gamma = \sqrt[2]{1 - \left(\frac{Z}{n\alpha}\right)^2}$ is derived by using $\frac{v}{c} = \frac{Z}{n\alpha}$ in $\gamma = \sqrt{1 - \frac{v^2}{c^2}}$. Here, Z is the atomic number of the atom, n is the principal quantum number, γ is the Lorentz factor, and α is the fine structure constant or Sommerfeld constant. The renormalized spin-orbit coupling parameter expression is given as:

$$\epsilon = \frac{2\Delta}{l}\left(1 - \frac{\gamma^3}{\gamma+1}\right) \quad ..Eq(6)$$

Here Δ is the SO splitting from atomic calculations with SOC relativistic corrections at ZORA level, two-component relativistic approximation to Dirac equation; and l is the angular quantum number for respective shells, and ϵ is the renormalized spin-orbit coupling constant. Table S1 (SI) contains the calculated SOC parameters throughout the periodic table and a detailed derivation is provided in the Supporting Information.

Computational Details of the Benchmark Calculations. Geometries were optimized using ANCopt method in GFN1-xTB framework at optimization level *tight* as implemented in xTB package. We also optimized the geometries at the DFT level with ZORA scalar relativistic

corrections for a consistent benchmarking reference. We used all electron approach with TZ2P quality of basis set in conjugation with GGA-PBE exchange-correlational functional.

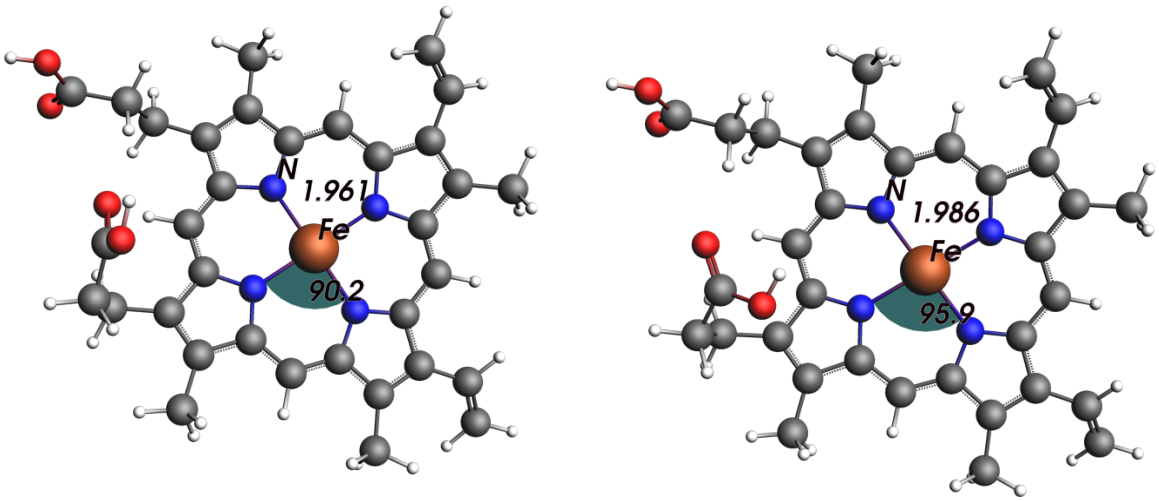

DFT **GFN1-xTB**

Figure 1. Optimized geometric parameters - bond distances and bond angles at DFT and GFN1-xTB levels, respectively, for heme moiety of hemoglobin.

Geometries.

Very small differences were found between the optimized geometries at GFN1-xTB and DFT levels. There are small differences in bond distances of ~0.01-0.03 Å and in bond angles ~2-5° going from DFT to GFN1-xTB (SI Section 3 for details). As example, Figure 1 shows these differences in bond distances and bond angles for heme moiety of hemoglobin. As expected, incorporation of SOC has only a marginal effect on geometries of the structures with change in bond distances and bond angles of ~10^{-3} and ~0.2-0.5°, respectively. Therefore, in the forthcoming, single-point SOC calculations in GFN1-xTB, termed as SOC-GFN1-xTB, were performed in the LS coupling model through our parametrization using the SOC parameters, as given in Table 1. For validation of results from GFN1-xTB, we performed single-point calculations at DFT level employing AMS-ADF software. We used GGA-PBE exchange-correlation functional with SOC-ZORA relativistic corrections. All electron approach with basis set of TZ2P quality was used.

Effect of SOC on Charge Transport Properties of Chromophores in MOFs. We reproduced the results of the effect of SOC on absorption spectra of the ions $M(bpy)_3^{2+}$ (M = Fe, Ru, Os; bpy = 2,2'-bipyridine) given their importance in the dipole-dipole energy transfer in MOFs as reported by Chakraborty et al.[17] In this reference work, SO splitting parameter λ of Ru(III), Fe(III), and Os(III) was reported as 1200, 440, and 3000 cm^{-1}, respectively, and matches well with the SOC-GFN1-xTB results, which yield values for λ= 1154, 561, and 3555 cm^{-1}, respectively. Following the same MO model as reported in the literature we calculated the absorption spectra of the above complexes. The absorption spectra at SOC-GFN1-xTB level, in combination with MO model from the literature (SOC-GFN1-xTB MO model), matches very well with the reference spectra (Figure 2.).

In the literature the $d\pi \rightarrow \pi^*$ electronic transitions from $d\pi$ orbitals (with T_{2g} symmetry) of the metal center to π^*_1 orbital of the bipyridine ligands were described with MO theory. In this scheme, relative energies of the excited states and ground states were reported in terms of parameters as in Δ, Γ, K, and λ (Table 1). Here, Δ is the energy difference between the $d\pi_E$ and $d\pi_{A_1}$ orbitals generated after lifting the degeneracy of the $d\pi$ orbitals. Similarly, Γ is the energy difference between the π^*_{1E} and $\pi^*_{1A_2}$ orbitals generated after lifting the degeneracy of the π^*_1 orbitals. K is the destabilizing energy of the metal-ligand coupled electronic state relative to the energy of the uncoupled state, and λ is the SOC constant. It is, in principle, possible to calculate these parameters within GFN1-xTB. For illustration, we calculated the Γ and K values from GFN1-xTB method. While we found a deviation of less than 40 cm^{-1} in K values in comparison to experimental data, the Γ values show large deviations of ~400-500 cm^{-1} for Fe and Os complexes. We attribute this deviation to the fact that GFN1-xTB is not fitted for yielding excellent structures. For some peaks, even deviations of 1000 cm^{-1} are observed. Therefore, we recommend the reference MO model, where the electronic structure parameter is fitted to experimental data.

Table 1. Parameters for the calculation of absorption spectra. All values are in cm^{-1}

	$Fe(bpy)_3^{2+}$		$Ru(bpy)_3^{2+}$		$Os(bpy)_3^{2+}$	
	Electronic MO Model [15]	**SOC-GFN1-xTB MO Model**	**Electronic MO Model[15]**	**SOC-GFN1-xTB MO Model**	**Electronic MO Model [15]**	**SOC-GFN1-xTB MO Model**
Δ	100	185	500	585	800	888
Γ	-1500	-1500	-1600	-1600	-2100	-2100
K	800	800	850	850	850	850
λ	440	561	1200	1154	3000	3555

The coupling between the promoted electron in a ligand localized orbital and metal center localized d^5 electron results in 12 orbitals with E, 6 orbitals with A_1, and 6 orbitals with A_2 symmetry. The MO scheme given in the literature then gives the matrices for effect of SOC in basis of these coupled states. Transitions from the ground state of A_1 symmetry to states of E symmetry are XY polarized and transitions to A_2 symmetry states are Z polarized. Table 2 gives the values of the electronic transitions for the complexes. Mean absolute deviations (MAD) were also calculated for each complex in SOC-GFN1-xTB approach as well as in reference MO model. The reference MO model shows MAD of 898.75, 1089.17, and 2024.72 while SOC-GFN1-xTB model gives MAD of 890.125, 1063.85, and 2226.00 for $Fe(bpy)_3^{2+}$, $Ru(bpy)_3^{2+}$, and $Os(bpy)_3^{2+}$ complex respectively. In Kober and Meier's approach, the peak intensity of Z polarized transitions could not be calculated. We followed the same procedure for reproducing the results and for an effective comparison. Figure 2 shows the spin-allowed electronic transitions for the complexes.

Table 2. Relative energy of $d\pi \rightarrow \pi^*$ electronic transitions calculated with SOC-GFN1-xTB MO model and Reference MO model for ions $M(bpy)_3^{2+}$ ($M = Fe, Ru, Os$; $bpy = 2,2' - Bipyridine$) with parameters from Table 1. Double prime symbols indicate excited states. σ is the standard deviation of peak values at SOC-GFN1-xTB model with respect to the reference MO model.

	$Fe(bpy)_3^{2+}$			$Ru(bpy)_3^{2+}$			$Os(bpy)_3^{2+}$		
Excitations	**Electronic MO Model[15]**	**SOC-GFN1-xTB**	**σ (SD)**	**Electronic MO Model[15]**	**SOC-GFN1-xTB**	**σ (SD)**	**Electronic MO Model[15]**	**SOC-GFN1-xTB**	**σ (SD)**
$1E''$	950	1060	77.78	1610	1676	46.67	2650	2989	239.7
$2E''$	-525	-518	4.950	35	70	24.75	1165	1381	152.7
$3E''$	-480	-335	102.5	250	312	43.84	1450	1816	258.8
$4E''$	-1025	-1153	90.51	-1495	-1426	48.79	-2965	-3343	267.3
$5E''$	-550	-439	78.48	10	76	46.67	450	789	239.7
$6E''$	-2025	-1914	78.48	-1565	-1529	25.46	-1135	-818	224.2
$7E''$	-2675	-2747	50.91	-3350	-3262	62.23	-5550	-5946	280.0
$8E''$	-2475	-2329	103.2	-2885	-2302	412.2	-4985	-3824	820.9
$9E''$	-1980	-1835	102.5	-1350	-1288	43.84	-750	-384	258.8
$10E''$	-645	-589	39.60	-415	-320	67.18	-115	-284	119.5
$11E''$	-2045	-1948	68.59	-1650	-1629	14.85	-1250	-842	288.5
$12E''$	-2525	-2577	36.77	-3095	-3026	48.79	-5165	-5543	267.3
$1A_1'$	-975	-796	126.6	-1285	-1190	67.18	-2785	-2957	121.6
$2A_1'$	855	701	108.9	1185	1089	67.88	2085	2153	48.08
$3A_1'$	-550	-438	79.19	10	76	46.67	450	789	239.7
$4A_1'$	-1980	-1835	102.5	-1350	-1288	43.84	-750	-384	258.8
$5A_1'$	-2025	-1914	78.48	-1565	-1529	25.46	-1135	-718	294.9
$6A_1'$	-2525	-2577	36.77	-3095	-3026	48.79	-5165	-5543	267.3
$1A_2'$	-1175	-1247	50.91	-1750	-1662	62.25	-3350	-3756	287.1

$\mathbf{2}A_2'$	-545	-447	69.29	-50	-29	14.89	950	1052	72.12
$\mathbf{3}A_2'$	-550	-438	79.19	10	76	46.67	450	789	239.7
$\mathbf{4}A_2'$	-1980	-1835	102.5	-1350	-1288	43.84	-750	-384	258.8
$\mathbf{5}A_2'$	-2025	-1914	78.48	-1565	-1529	25.46	-1135	-718	294.9
$\mathbf{6}A_2'$	-2525	-2577	36.77	-3095	-3026	48.79	-5165	-5543	267.3

227

228

229 An excellent agreement was observed between the reference spectra and the spectra obtained
230 at SOC-GFN1-xTB MO level. Figure 2 depicts the resemblances between the reproduced
231 literature and our work.

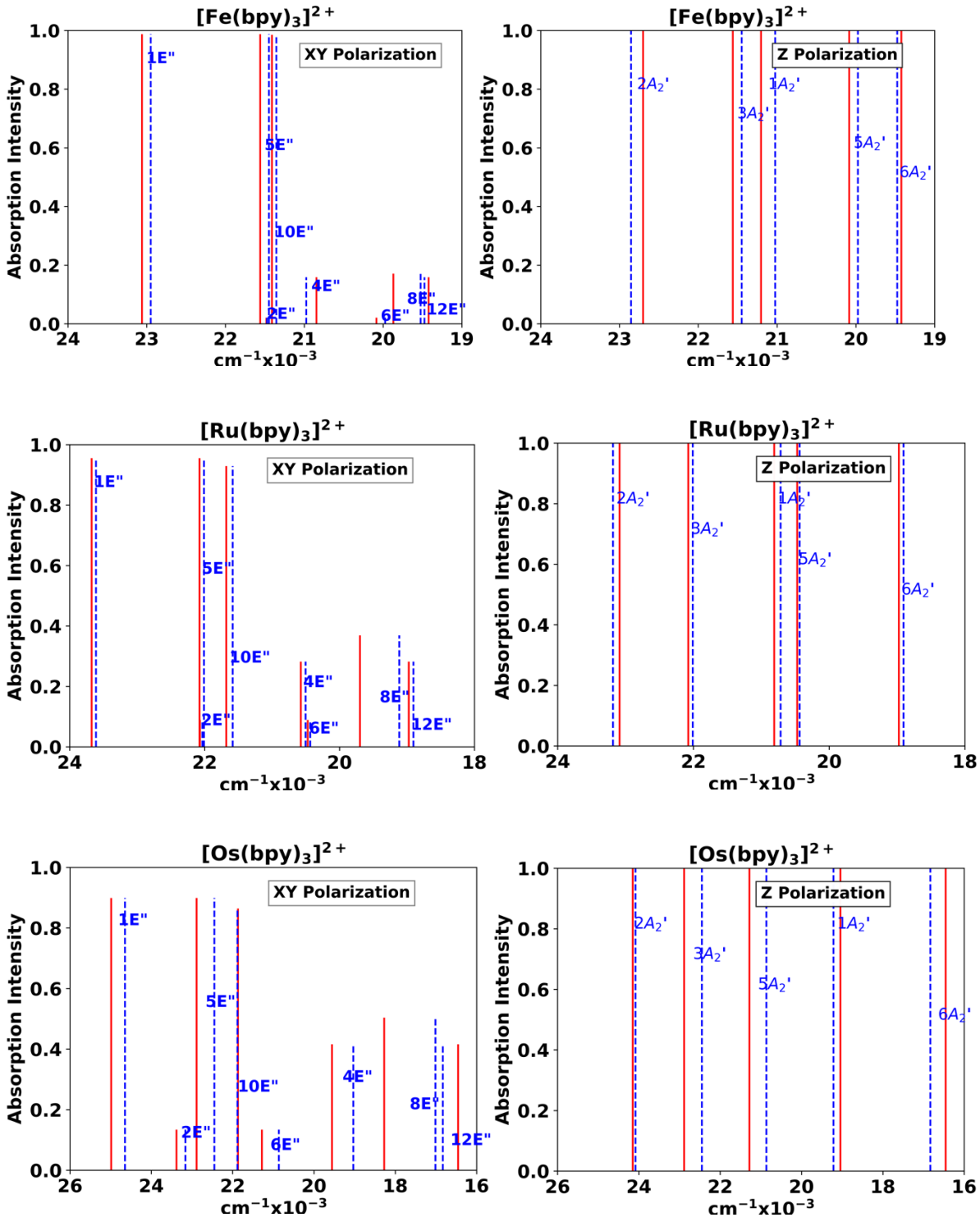

Figure 2. Absorption spectrum of $M(bpy)_3^{2+}$ $(M = Fe, Ru, Os; bpy = 2,2' - Bipyridine)$ complexes calculated at Reference MO model (blue dashed lines) and SOC-GFN1-xTB MO model (red lines) with system specific Δ, Γ, λ, and K values (table 2). XY and Z polarization are the polarization of $d\pi \rightarrow \pi^*$ electronic excitations.

Superatoms: $[WAu_{12}]$ is an icosahedral 18-valence electron (VE) superatom (Figure 3) with significant SO splitting of the electronic levels. Superatoms have an electronic configuration sequence quite different from the isolated atom, but resemble atom-like electronic and chemical behaviors. Here, the electronic configuration of the reference superatom is $1s^2,1p^6,1d^{10}$.

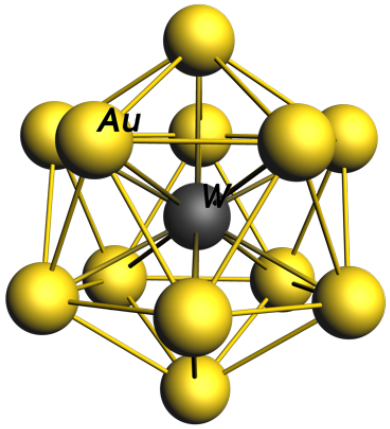

Figure 3. Optimized icosahedral (I_h) $[WAu_{12}]$ gold-based superatom.

Figure 4. depicts the SOC-imposed orbital splitting for DFT and GFN1-xTB. As most of the exciting chemistry revolves around the valence orbitals, we comparehere the HOMO d-orbitals of the clusters. SOC-GFN1-xTB gives an excellent match with SO splitting and electron affinity difference (ΔEA) compared to DFT calculatinos with SOC-ZORA. Electron affinity difference (ΔEA) is given as:

$$\Delta EA_{SOC-GFN1-xTB} = EA_{SOC-GFN1-xTB} - EA_{GFN1-xTB}$$

$$\Delta EA_{SOC-DFT} = EA_{SOC-DFT} - EA_{DFT}$$

Calculated SO splitting of HOMO d orbitals at DFT-SOC level is 28.0 meV, while SOC-GFN1xTB predicts the value of 29.5 meV. The ΔEA of the cluster in our model is estimated at 2.122 eV and matches very well with reported theoretical value 2.090 eV [21] as well as

experimental value of 2.020 eV [21]. Overall, we observe excellent agreement between experiment, DFT and SOC-GFN1-xTB.

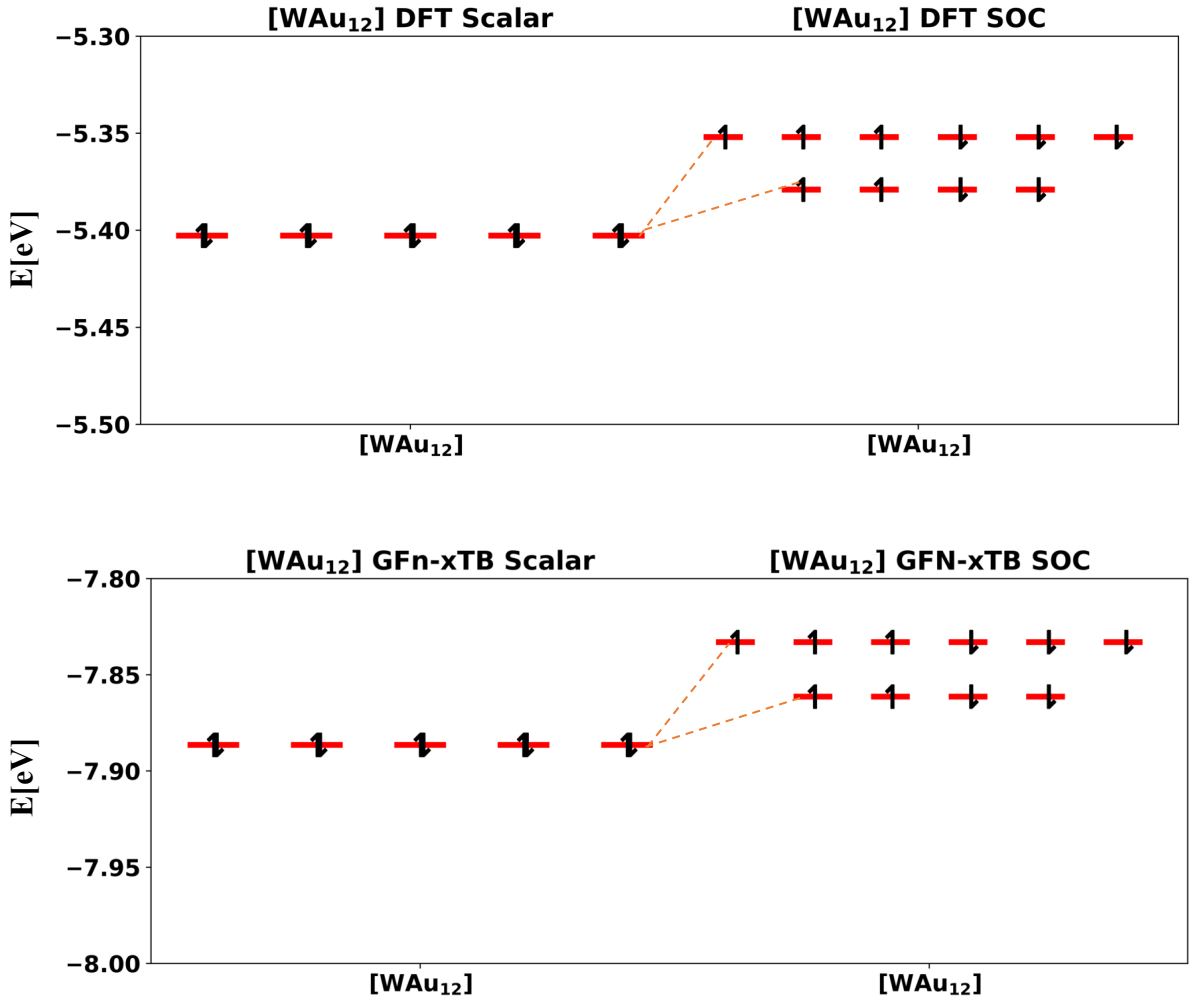

Figure 4. Spin-orbit splitting for icosahedral (I_h) $[WAu_{12}]$ calculated at SOC-GFN1-xTB level and at DFT-SOC with ZORA relativistic corrections. All values are in eV.

Effect of SOC on Binding of O_2 on Ferrous Deoxyheme.

Binding of O_2, a triplet state molecule, to quintet state molecule ferrous deoxyheme, is a vital process for life in its present form. Nature has used the complexes of transition metals to bind,

carry, and unload the O_2 to the cells. There are several factors which prove transition metals as the best candidate for the binding, and one crucial factor is SOC. Despite of small SOC in ferrous deoxyheme, the reaction proceeds ~10^{11} faster than in the non-biological Fe-O^+ system. Even though the major contribution to the binding process is based on the ligation of heme to Fe (II) center, which facilitates the low energy interval among different spin states as its quintet ground state and the triplet state of heme moiety differ in energy by about 10 kJ mol^{-1} at an Fe-O distance of 2.5 Å as in oxyheme, the SOC contribution is significant. It induces a spin flip from the quintet ground state of deoxyheme to the triplet state of deoxyheme. This lifts the spin restriction on the reaction, as now deoxyheme and dioxygen are both in triplet states. The starting oxyheme radical pair (Fe^{3+} O_2^-) is in a charge transfer state with triplet spin, which flips its spin state to singlet through SOC [32–34]. Understanding the effect of SOC on this binding process would assist mimicking the natural processes. Here, we have reported the values for SOC in both deoxyheme and oxyheme. We have calculated the SOC in our reference structure at SOC-GFN1-xTB level and compared it with the results reported in the literature. Mössbauer spectroscopy estimates the SOC ~0.8 kJ mol^{-1} [22,32] for ferrous deoxyheme in hemoglobin and myoglobin and a theoretical value of 0.96[34] kJ mol^{-1} for ferric oxyheme; our calculated values are 1.6 kJ mol^{-1} for ferry deoxymene and 1.2 kJ mol^{-1} respectively and matches reasonably well with the reported Mössbauer and theoretically predicted value.

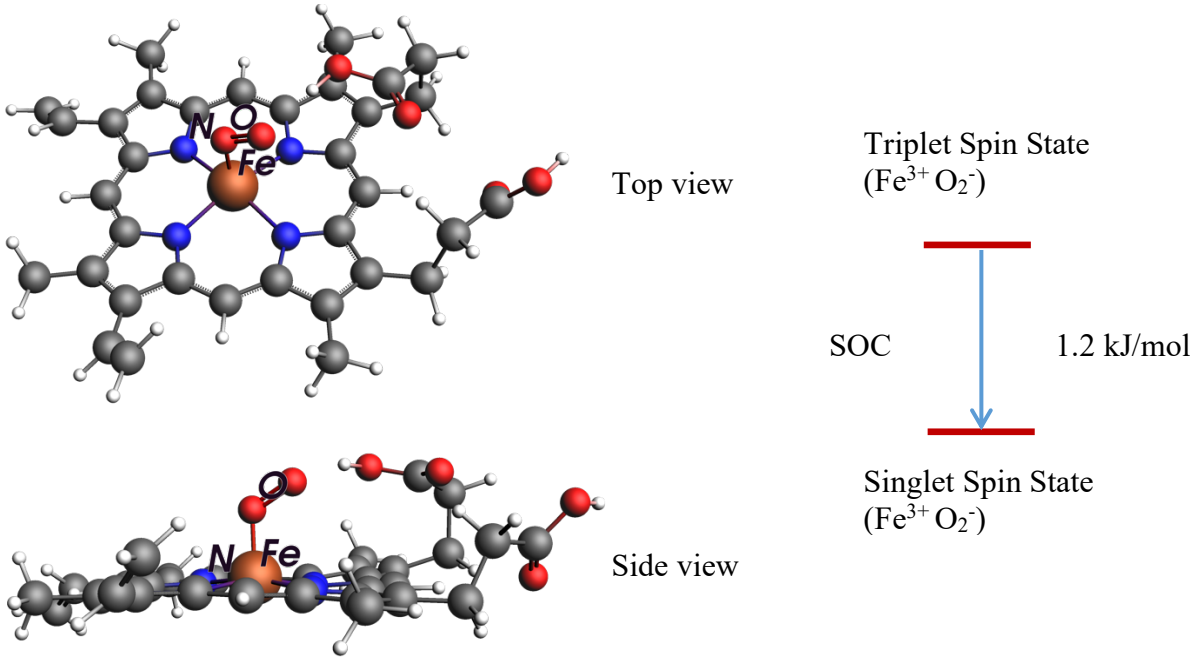

Figure 5. Optimized geometry of ferrous oxyheme at GFN1-xTB level and calculated SOC energy contribution to the spin flip of triplet (Fe^{3+} O_2^-) to singlet (Fe^{3+} O_2^-) radical at SOC-GFN1-xTB level.

Conclusions

We have discussed the parameterization and implementation formalism of SOC for the framework of GFN1-xTB and calculated parameters for the elements throughout the periodic table. We tested the SOC-GFN1-xTB formalism on the reference structures as in superatoms, transition metal containing heme moieties, and transition metal containing bipyridine complexes as chromophores in energy transfer processes in MOFs. We have used none of these systems for the calculation of the SOC parameters. The resulting SO splittings are in close accordance with DFT-based reference calculations as well as experiments, with deviations smaller than those that are expected for GFN1-xTB-obtained molecular orbitals. This shows excellent transferability and assures that these parameters will be very useful for a wide range of applications where SOC is important. Examples include studying energy transfer processes,

designing novel magnetic nanoclusters, and understanding the role of transition metal in spin catalysis and mimicking the natural catalysis processes.

With this work, it is now possible to incorporate SOC in all GFN-xTB calculations with far less computational costs compared to the SOC-ZORA DFT. This work also extends the availability of parameters throughout the periodic table which was limited to pre-calculation of the parameters for literature specific systems.

As GFN-xTB is a well-defined approximation to DFT, extensions to the Hamiltonian are system-independent and transferable within different implementations. Therefore, the presented parameters and implementation work well for various GFN-xTB extensions and implementations as in standalone GFN-xTB, AMS-GFN-xTB, and GFN-xTB in dftb+.

Our parameters are available at GitHub for the incorporation of spin-orbit coupling for GFN-xTB implementations beyond the presented model. (https://github.com/gajh494c/SOC-DFTB).

ASSOCIATED CONTENT

Supporting Information. Detailed information on the Spin-Orbit coupling parameters, and geometric parameters of all crystal structures considered in this work. This material is available free of charge.

AUTHOR INFORMATION

Corresponding Author

*Email: Thomas.Heine@tu-dresden.de

Notes

The authors declare no competing financial interest.

ACKNOWLEDGEMENT

We thank the Center for Information Services and High-Performance Computing (ZIH) at TU Dresden for computational resources, and CRC 1415 as well as SPP 2244 for financial support.

REFERENCES:

1. W. Koch and M. C. Holthausen, *A Chemist's Guide to Density Functional Theory* (Wiley, 2001).

2. R. O. Jones, Reviews of Modern Physics **87**, 897 (2015).

3. C. Bannwarth, S. Ehlert, and S. Grimme, Journal of Chemical Theory and Computation **15**, 1652 (2019).

4. S. Grimme, C. Bannwarth, and P. Shushkov, Journal of Chemical Theory and Computation **13**, 1989 (2017).

5. M. Bursch, A. Hansen, and S. Grimme, Inorganic Chemistry **56**, 12485 (2017).

6. A. B. Kanj, J. Bürck, N. Vankova, C. Li, D. Mutruc, A. Chandresh, S. Hecht, T. Heine, and L. Heinke, Journal of the American Chemical Society **143**, 7059 (2021).

7. C. Bannwarth, E. Caldeweyher, S. Ehlert, A. Hansen, P. Pracht, J. Seibert, S. Spicher, and S. Grimme, WIREs Comput Mol Sci **11** (2021).

8. C. Köhler, T. Frauenheim, B. Hourahine, G. Seifert, and M. Sternberg, Journal of Physical Chemistry A **111**, 5622 (2007).

9. G. Jha and T. Heine, Journal of Chemical Theory and Computation **18**, 4472 (2022).

10. E. van Lenthe, J. G. Snijders, and E. J. Baerends, Journal of Chemical Physics **105**, 6505 (1996).

11. E. van Lenthe, E. J. Baerends, and J. G. Snijders, The Journal of Chemical Physics **99**, 4597 (1998).

12. W. Liu, Molecular Physics **108**, 1679 (2010).

13. C. Köhler, T. Frauenheim, B. Hourahine, G. Seifert, and M. Sternberg, Journal of Physical Chemistry A **111**, 5622 (2007).

14. S. K. Lower and M. A. El-Sayed, Chem. Rev. **66**, 199 (1966).

15. E. M. Kober and T. J. Meyer, Inorganic Chemistry **21**, 3967 (1982).

16. E. M. J. Johansson, M. Odelius, S. Plogmaker, M. Gorgoi, S. Svensson, H. Siegbahn, and H. Rensmo, J. Phys. Chem. C **114**, 10314 (2010).

17. A. Chakraborty, S. Ilic, M. Cai, B. J. Gibbons, X. Yang, C. C. Slamowitz, and A. J. Morris, J. Am. Chem. Soc **142**, 1 (2020).

18. A. W. Castleman and S. N. Khanna, J. Phys. Chem. C **113**, 2664 (2009).

19. E. A. Doud, A. Voevodin, T. J. Hochuli, A. M. Champsaur, C. Nuckolls, and X. Roy, Nat Rev Mater **5**, 371 (2020).

20. J. U. Reveles, P. A. Clayborne, A. C. Reber, S. N. Khanna, K. Pradhan, P. Sen, and M. R. Pederson, Nature Chemistry **1**, 310 (2009).

21. A. Muñoz-Castro and R. Arratia-Perez, Physical chemistry chemical physics : PCCP **14**, 1408 (2012).

22. K. P. Jensen and U. Ryde, The Journal of biological chemistry **279**, 14561 (2004).

374 23. B. F. Minaev and H. Ågren, Collect. Czech. Chem. Commun. **60**, 339 (1995).

375 24. C. M. Marian, WIREs Comput Mol Sci **2**, 187 (2012).

376 25. A. L. Buchachenko and V. L. Berdinsky, Chem. Rev. **102**, 603 (2002).

377 26. K. Ohno, Theoret. Chim. Acta **2**, 219 (1964).

378 27. G. Klopman, Journal of the American Chemical Society **86**, 4550 (1964).

379 28. S. Grimme, The Journal of Chemical Physics **138**, 244104 (2013).

380 29. Zeitschrift für Physikalische Chemie **12**, 335 (1957).

381 30. B. Hourahine, B. Aradi, V. Blum, F. Bonafé, A. Buccheri, C. Camacho, C. Cevallos,
382 M. Y. Deshaye, T. Dumitrică, A. Dominguez, S. Ehlert, M. Elstner, T. van der Heide, J.
383 Hermann, S. Irle, J. J. Kranz, C. Köhler, T. Kowalczyk, T. Kubař, I. S. Lee, V. Lutsker, R. J.
384 Maurer, S. K. Min, I. Mitchell, C. Negre, T. A. Niehaus, A. M. N. Niklasson, A. J. Page, A.
385 Pecchia, G. Penazzi, M. P. Persson, J. Řezáč, C. G. Sánchez, M. Sternberg, M. Stöhr, F.
386 Stuckenberg, A. Tkatchenko, V. W.-Z. Yu, and T. Frauenheim, The Journal of Chemical
387 Physics **152**, 124101 (2020).

388 31. G. Te Velde and E. J. Baerends, Physical Review B **44**, 7888 (1991).

389 32. H. Eicher, D. Bade, and F. Parak, Journal of Chemical Physics **64**, 1446 (1976).

390 33. H. Eicher and A. Trautwein, Journal of Chemical Physics **50**, 2540 (1969).

391 34. B. F. Minaev and V. A. Minaeva, 1814-9758 (2008).

392